# Photoacoustic Speckle and Spectral analysis of Vasculature Trees

M. N. Fadhel[1] and M. C. Kolios[1]

[1] Ryerson University/Department of Physics, Toronto, Canada

*Abstract*—**This paper discusses the use of ultrasound tissue characterization methods to photoacoustic (PA) data to differentiate between tissues with different vasculature structures. The dominant source responsible for ultrasound scattering in soft tissues (including tumors) is not well known in pulse echo ultrasound. PA imaging is based on the detection of ultrasound waves generated by optical absorption. Since the hemoglobin in blood dominates the absorption of light in soft tissues (at particular laser wavelengths), the PA signal is dominated by the contribution of the vasculature. Organized and chaotic vasculature trees were simulated using a fractal model to represent normal and tumor vasculature, respectively. The generated PA signals from these vascular were simulated through the solution of the photoacoustic wave equation using the Green's function approach. Ultrasound resolution PA signals generated were detected by simulating a 256 element transducer with a 10-50 MHz bandwidth. Reconstructed images were acquired using a delay and sum method. Image analysis was performed by fitting the image probability density functions (PDF) of Rayleigh, Nakagami (NG), and Generalized Gamma (GG) distributions to the histogram of the reconstructed images. The speckle sizes of the reconstructed PA images were calculated using autocovariance. Spectrum analysis of the ultrasound frequency components of the photoacoustic signals was performed by linear regression analysis of the power spectrums of the radiofrequency (RF) data, as done in conventional ultrasound tissue characterisation. The results suggest that the Rayleigh, NG distributions, and the power spectrum regression analysis can be used to differentiate between the simulated normal and tumor vasculatures. The changes in these parameters correlate to a higher density of tumor vasculatures than normal vasculatures.**

*Keywords*— **Photoacoustic, vasculature tree, tumor, speckle analysis, spectral analysis.**

## I. Introduction

Analysis of unresolved structures in ultrasound pulse echo imaging has been studied extensively in tissue characterization to differentiate between normal and tumor tissues [1]–[4]. The tissue characterization parameters from these studies correlated to the shape and number density of the particles generating the scattered waves (the scattering sources). Due to the low ultrasound contrast in soft tissues [3], many biological structures contribute to scattering. Therefore, it is difficult to attribute a dominant scattering source to particular biological structures such as the nucleus; this increases uncertainty in the interpretation of the parameters derived in tissue characterization. In photoacoustic (PA) imaging, the formation of ultrasound waves is due to the absorption of light. Blood vessels have an optical absorption coefficient up to six orders of magnitude larger than the surrounding tissues (which is highly dependent on the optical irradiation wavelength), which makes vessels the dominant ultrasound source [5].

The tumor micro-environment is unique when compared to that of normal tissues [6]. This unique environment supports angiogenesis; the formation of new blood vessels. The tumor vascular structure is different compared to that of normal tissue. Tumor vasculatures are disorganized, twisted and uneven with unusual branching patterns. In contrast, normal vasculatures are well organized and evenly distributed [7]. It is the purpose of this work to demonstrate that image analysis of the unresolved structures in PA images, as well as conventional ultrasound tissue characterization methods can be used to probe the vascular structure.

The analysis of the PA data can be performed in time or frequency domain. Envelop statistics is a time-domain analysis performed by fitting the histogram of an image to a probability density function (PDF). The fitted parameters can depend on the size, density and organization of the wave sources. The Rayleigh distribution is a commonly used PDF which assumes large number of randomly located wave sources [8]. The $\sigma$ parameter is calculated from the Rayleigh distribution, and it is related to the size and concentration of the wave sources. The Nakagami (NG) and Generalized Gamma (GG) distributions are other PDFs have been used in tissue characterization to overcome the assumptions in Rayleigh distribution [2], [9], [10]. The NG distribution is used to calculate two parameters: the shape parameter (m) takes into account low concentration and organization, and the scaling parameter ($\Omega$) which is the average power of the signals. The GG distribution is used to calculate a scale parameter (a) which is the mean of the PDF and the shape parameter (c/v) which correlates to the effective number of the wave source.

Spectral analysis fit a function to the calculated power spectrum of the signal [4], [11]. Due to the specific bandwidth of the transducer, a linear fitting function is widely used. The parameters calculated from the linear fit are the slope, y-intercept, and mid-band fit (MBF); the slope mainly correlates to the size of the PA absorbers, the y-intercept correlates to the concentration of the PA absorbers, and MBF can be calculated from the slope and the y-intercept.

In ultrasound resolution PA imaging analysis of the signal generated from the unresolved vasculatures has the potential to differentiate between normal and tumor vasculatures. This can be used either for early tumor detection and treatment monitoring. The main objective of the study is to test different signal analysis techniques on simulated PA images of non-resolved vasculatures to evaluate their potential in characterizing vascular tissues, such as cancer.

## II. Material and Methods

### *A. Generation of the vascular trees*

The vascular trees were generated using a fractal model [12]. To generate the fractal model, two cylinders are designated as the parent segments located at [0, 0, 0] mm, which bifurcate to generate the daughter segments. This pattern was repeated 12 times to generate vascular trees. The tree had an initial diameter of 0.80 mm and a final diameter of 0.06 mm. The parameters used for normal vasculature are 0.95 for the bifurcation index, 0.9 for distance factor, 25° to 27° for branching angle and 0-2π for branching orientation. Parameters for tumor vasculatures are the same except the branching angle. The branching angle was replaced with a random value within the range of 25° to 140°. Four normal and four tumor vasculatures were simulated, and one of each are presented in fig.1.

### *B. Calculate the photoacoustic signals*

The photoacoustic pressure waves were calculated from the solution of the photoacoustic wave equation using the Green's function approach [13]. The generated pressure ($p(r,t)$) at location $r$ and time $t$ from a short laser pulse is:

$$p(r,t) = \frac{1}{4\pi v_s^2}\frac{\partial}{\partial t}\left[\frac{1}{v_s t}\int dr' p_0(r')\delta\left(t - \frac{|r - r'|}{v_s}\right)\right]$$

where $v_s$ is the speed of ultrasound in the medium (1500 m/s), $r'$ is the location of the absorber, and $p_0$ is the pressure profile after the laser excitation (directly correlated to the optical absorption coefficient). The initial pressure $p_0$ was simulated to be 1 at the vessel location and 0 for surrounding tissues. 256 pressure profiles were acquired at locations from [-7, 0, 15] mm to [7, 0, 15] mm with spacing of 0.055 mm.

### *C. Image Reconstruction*

An image was reconstructed for each vasculature tree using the 256 pressure profiles generated from the previous step. A Butterworth bandpass filter of order 3 and 10 MHz to 50 MHz was used on each pressure profile to account for the transducer bandwidth. The images were reconstructed using the conventional delay and sum for every 64 elements (as is done for commercial PA scanners). In the delay and sum, each signal was multiplied by sin (θ) where θ is the angle to the vertical line. This is done to account for the transducer directivity. Apodization was applied by multiplying the 256 elements with a hamming filter.

### *D. Speckle analysis*

Windows of dimensions of 2.3x2.3 mm were selected on the reconstructed images as shown in fig. 2. Rayleigh [8], NG [2] and GG [10] PDFs were fitted on the calculated histograms of the selected windows using the maximum likelihood estimate (MLE) technique.

The horizontal and vertical average speckle sizes of the selected windows were calculated using the image autocovariance. The autocovariance in the axial and lateral direction were calculated and averaged. The results were fitted to a Gaussian to determine the full width half maxima which represent the speckle size. The parameters for normal and tumor vasculatures were compared using a two sample t-test.

### *E. Spectral analysis*

The average power spectrum of the radiofrequency (RF) signals in ROI were acquired by calculating the power spectrum of each RF line and averaging them. The average power spectrum was fitted using linear regression analysis, with the frequency range of 10 MHz to 50 MHz. The slope, MBF and y-intercept parameters were calculated from the fitted line [11]. The three parameters were compared for normal and tumor vascular structures using a two sample t-test.

## III. Results

### A. Vasculature trees and reconstructed images

Typical normal and tumor vascular trees are presented in fig. 1. The normal vasculature is more organized and less chaotic when compared to tumor vasculature. The reconstructed PA images of the same vasculature trees in fig. 1 are presented in fig.2. These images take into account transducer apodization, directivity, and bandwidth.

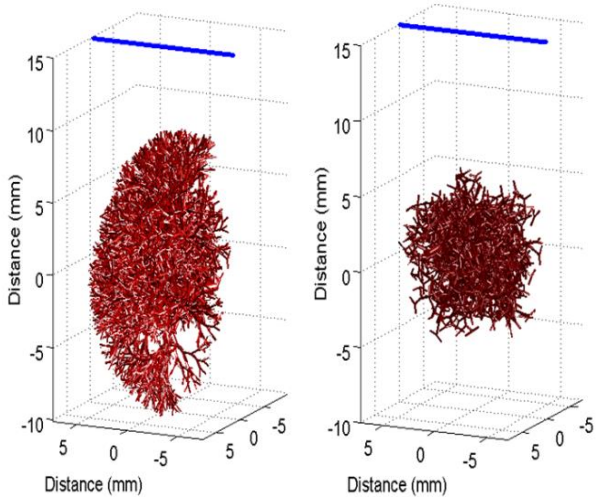


a) b)

Fig. 1 Simulated vascular trees using a fractal model for (a) the normal vasculature with branching angle ranges between 25-27° and (b) the tumor vasculature with branching angle ranges between 25-140°. The blue dotted line represents the location of the simulated point detectors.

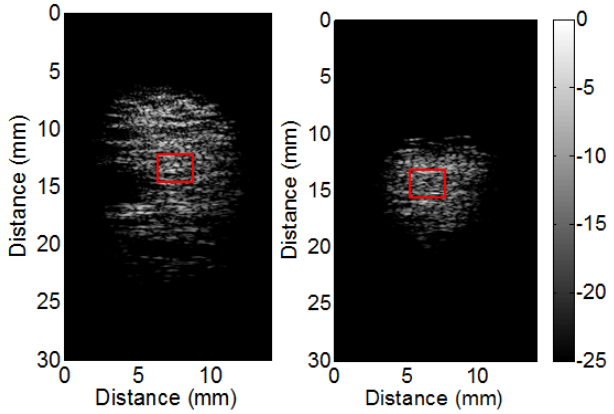


Fig. 2 Reconstructed images of the simulated vasculature tree in fig. 1 (a) and (b). The red square represents the selected window used for image and signal analysis. The gray scale bar is amplitude in decibels (dB).

### B. Speckle and spectral parameters

The parameters acquired by fitting the PDF of Rayleigh, NG and GG distributions to the windowed images of the reconstructed vasculatures are shown in table 1. The two parameters which demonstrate a difference between the reconstructed images of normal and tumor vasculatures are the σ in Rayleigh distribution and Ω in NG distribution.

The auto-covariance approach, used to determine the speckle size parameters, was unable to differentiate between normal and tumor vasculatures. The average horizontal and vertical speckle sizes were 0.220 ± 0.010 mm and 0.1223 ± 0.011 mm for normal vasculatures, and 0.227 ± 0.015 mm and 0.108 ± 0.019 mm for tumor vasculature with p- value of 0.505 and 0.284 respectively.

The results for spectral analysis, using the linear regression method are provided in table 2. The two parameters which demonstrate a difference between the reconstructed images of normal and tumor vasculatures are the y- intercept and MBF.

Table 1 The average PDF parameters trees using Rayleigh, NG and GG distributions for the reconstructed images of 4 normal and 4 tumor simulated vasculature trees

| | Parameter | Normal | Tumor | p-value |
|---|---|---|---|---|
| Rayleigh PDF | σ | 0.097 ± 0.051 | 0.192 ± 0.030 | 0.019* |
| NG PDF | m | 0.951 ± 0.034 | 1.147 ± 0.160 | 0.053 |
| | Ω | 0.023 ± 0.020 | 0.074 ± 0.020 | 0.014* |
| GG PDF | a | 0.013 ± 0.016 | 0.118 ± 0.110 | 0.108 |
| | c/v | 0.111 ± 0.081 | 0.590 ± 0.606 | 0.168 |

Table 2 Calculated spectral parameters for the reconstructed photoacoustic images of normal and tumor simulated vasculature trees

| | Normal | Tumor | p-value |
|---|---|---|---|
| Slope (dB/MHz) | -0.926 ± 0.021 | -0.952 ± 0.022 | 0.202 |
| y-Intercept (dB) | 20.38 ± 2.46 | 25.43 ± 1.31 | 0.013* |
| MBF (dB) | -7.41 ± 2.55 | -3.12 ± 1.49 | 0.032* |

## IV. Discussion

The difference in the organization of normal and tumor vasculatures can be seen in fig. 1. The normal vasculature occupies a larger volume when compared to tumor vasculature. This suggests an increase in the vascular density of tumor, which has been observed experimentally [14]. Figure 2 provides the reconstructed images of vasculature trees using an ultrasound transducer of 256 elements and 10-50 MHz bandwidth. In the images we are unable to resolve individual blood vessels. The images result in a speckle pattern.

For the analysis of the envelope statistics, the Rayleigh and NG PDFs were able to differentiate between the vasculatures based on the fit parameters. From table 1, all calculated parameters increased for tumor tissues, but only two parameters ($\sigma$ and $\Omega$) were significantly higher. The $\Omega$ parameter had the lowest p-value (0.014). Using the fit parameters to the GG distribution we are unable to differentiate between the two vascular structures. For NG and GG distributions the scale parameters ($\Omega$ and a) were better in differentiating the vasculatures than the shape parameters (m and c/v). The higher concentration of tumor vasculature could explain the increase in the scale parameters. For speckle size analysis, the results were unable to differentiate between normal and tumor vasculatures.

Spectral analysis was able to differentiate between normal and tumor vasculatures (table 2) by the y-intercept given the p-value of 0.013. Assuming randomly distributed absorbers, the significant increase in the y-intercept parameter could be correlated to an increase of the absorber density for tumor vasculatures. The MBF was also able to different between the two vasculatures as it is correlated to the y-intercept. The slope was unable to differentiate between the vasculatures as it correlates to the size of the absorber.

## V. Conclusion

This research demonstrates the potential of applying speckle and spectral analysis on photoacoustic images to detect structural changes of vasculatures. Normal and tumor vasculature have different structural distributions. The best parameters to differentiate between these structural changes are $\sigma$ for Rayleigh PDF, $\Omega$ for NG PDF, and y-intercept and MBF for linearly fitting the power spectrum. Better understanding of these parameters can improve photoacoustic modality in detecting and treatment monitoring of tumor.

## Acknowledgment

I would like to thank Eno Hysi, Jason Zalev and Behnaz Pourebrahimi for helping me to complete these simulations. This word was funded through grants made available by the Natural Sciences and Engineering Research Council of Canada (NSERC), and Terry Fox Foundation (TFF).

## Conflict of Interest

I declare there is no conflict of interest.

## References

[1] A. S. Tunis, G. J. Czarnota, A. Giles, M. D. Sherar, J. W. Hunt, and M. C. Kolios, "Monitoring structural changes in cells with high-frequency ultrasound signal statistics," *Ultrasound Med. Biol.*, vol. 31, no. 8, pp. 1041–1049, Aug. 2005.

[2] P. Mohana Shankar, "A general statistical model for ultrasonic backscattering from tissues," *IEEE Trans. Ultrason. Ferroelectr. Freq. Control*, vol. 47, no. 3, pp. 727–736, May 2000.

[3] J. Mamou and M. L. Oelze, Eds., *Quantitative ultrasound in soft tissues*. Dordrecht: Springer, 2013.

[4] M. C. Kolios, G. J. Czarnota, M. Lee, J. W. Hunt, and M. D. Sherar, "Ultrasonic spectral parameter characterization of apoptosis," *Ultrasound Med. Biol.*, vol. 28, no. 5, pp. 589–597, May 2002.

[5] J. Yao and L. V. Wang, "Photoacoustic tomography: fundamentals, advances and prospects," *Contrast Media Mol. Imaging*, vol. 6, no. 5, pp. 332–345, Oct. 2011.

[6] R. K. Jain, "Taming Vessels to Treat Cancer," *Sci. Am.*, vol. 18, pp. 64–71, 2008.

[7] M. A. Konerding, E. Fait, and A. Gaumann, "3D microvascular architecture of pre-cancerous lesions and invasive carcinomas of the colon," *Br. J. Cancer*, vol. 84, no. 10, pp. 1354–1362, May 2001.

[8] J. W. S. B. Rayleigh, *On the Resultant of a Large Number of Vibrations of the Same Pitch and Arbitrary Phase*. 1880.

[9] P. M. Shankar, "Ultrasonic tissue characterization using a generalized Nakagami model," *IEEE Trans. Ultrason. Ferroelectr. Freq. Control*, vol. 48, no. 6, pp. 1716–1720, Nov. 2001.

[10] E. W. Stacy, "A Generalization of the Gamma Distribution," *Ann. Math. Stat.*, vol. 33, no. 3, pp. 1187–1192, Sep. 1962.

[11] F. L. Lizzi, M. Greenebaum, E. J. Feleppa, M. Elbaum, and D. J. Coleman, "Theoretical framework for spectrum analysis in ultrasonic tissue characterization," *J. Acoust. Soc. Am.*, vol. 73, no. 4, pp. 1366–1373, Apr. 1983.

[12] J. Zalev, "Detection and monitoring for cancer and abnormal vasculature by photoacoustic signal characterization of structural morphology." .

[13] L. V. Wang, "Tutorial on Photoacoustic Microscopy and Computed Tomography," *IEEE J. Sel. Top. Quantum Electron.*, vol. 14, no. 1, pp. 171–179, 2008.

[14] N. Weidner, J. P. Semple, W. R. Welch, and J. Folkman, "Tumor Angiogenesis and Metastasis — Correlation in Invasive Breast Carcinoma," *N. Engl. J. Med.*, vol. 324, no. 1, pp. 1–8, Jan. 1991.